Molecular sieving of linear and branched C6 alkanes by tannin-derived carbons

Jimena Castro-Gutiérrez, Erika de Oliveira Jardim, Rafael Luan Sehn Canevesi, Joaquin Silvestre-Albero, Martin Kriesten, Matthias Thommes, Alain Celzard, Vanessa Fierro

▶ **To cite this version:**

Jimena Castro-Gutiérrez, Erika de Oliveira Jardim, Rafael Luan Sehn Canevesi, Joaquin Silvestre-Albero, Martin Kriesten, et al.. Molecular sieving of linear and branched C6 alkanes by tannin-derived carbons. Carbon, 2021, 174, pp.413-422. 10.1016/j.carbon.2020.12.061 . hal-03091665

HAL Id: hal-03091665
https://hal.univ-lorraine.fr/hal-03091665v1

Submitted on 2 Mar 2021

HAL is a multi-disciplinary open access archive for the deposit and dissemination of scientific research documents, whether they are published or not. The documents may come from teaching and research institutions in France or abroad, or from public or private research centers.

L'archive ouverte pluridisciplinaire **HAL**, est destinée au dépôt et à la diffusion de documents scientifiques de niveau recherche, publiés ou non, émanant des établissements d'enseignement et de recherche français ou étrangers, des laboratoires publics ou privés.

Distributed under a Creative Commons Attribution - NonCommercial - NoDerivatives 4.0 International License

Molecular sieving of linear and branched C_6 alkanes by tannin-derived carbons

Jimena Castro-Gutiérrez,[a] Erika De Oliveira Jardim,[b] Rafael Luan Sehn Canevesi,[a] Joaquin Silvestre-Albero,[b] Martin Kriesten,[c] Matthias Thommes,[c] Alain Celzard[a] and Vanessa Fierro[a]*

[a] Université de Lorraine – CNRS – Institut Jean Lamour, 27 Rue Philippe Séguin, 88051 Epinal, France

[b] Laboratorio de Materiales Avanzados, Departamento de Química Inorgánica-IUMA, Universidad de Alicante, Carretera San Vicente del Raspeig-Alicante s/n, E-03690 San Vicente del Raspeig, Spain

[c] Institute of Separation Science and Technology, Friedrich-Alexander-Universität Erlangen-Nürnberg, Egerlandstr. 3, 91058 Erlangen, Germany

Corresponding author's e-mail: vanessa.fierro@univ-lorraine.fr

Abstract

Two micro-mesoporous carbons (MMCs): a disordered mesoporous carbon (DMC) and an ordered mesoporous carbon (OMC), synthesized by an easy, low-cost, and green method are proposed as efficient hydrocarbon sieves for the separation of C_6 isomers: *n*-hexane (nHEX), 2-methylpenthane (2MP) and 2,2-dimethylbutane (22DMB). Their textural characterization reveals a highly interconnected pore network within the DMC, while a reverse hierarchy of ordered mesopores only accessible through narrow micropores is found in the OMC. The pore texture strongly affects their adsorption performance by kinetic and molecular sieving effects; the narrow constrictions in the OMC allow adsorption of nHEX and partially 2MP but not 22DMB, whereas the highly connected pore network of DMC allows adsorption of the three isomers. Multi-component adsorption isotherms calculated from the single-component experimental results by ideal adsorbed solution theory (IAST) demonstrates that the OMC material has a remarkably high selectivity for the adsorption of nHEX and nHEX + 2MP from binary and ternary mixtures, respectively. To the best of the authors' knowledge, such behavior has never been reported so far for carbon materials. Hence, this study shows that tannin-derived MMCs have great potential to be used as an eco-friendly and low-cost alternative for the selective separation of di-branched C_6 isomers.

Keywords: alkane separation, micro-mesoporous carbons, tannins, molecular sieves

1. Introduction

Higher-quality gasoline is obtained when di-branched alkanes with 5 to 7 carbon atoms (C_5 – C_7) are present because they increase the octane number, and consequently the performance of the fuel in the engine [1,2]. In this regard, oil refining includes a step of catalytic isomerization of linear hydrocarbons to increase the amount of di-branched alkanes in gasoline. However, the limitations of the process result in incomplete reactions, leading to a mix of linear, mono- and di-branched alkanes [2]. Therefore, it is very important to be able to separate the di-branched iso-alkanes from the rest of the blend to increase the quality of gasoline, and to recycle the linear and mono-branched isomers into the isomerization reactor [1]. For this purpose, molecular sieves are of great industrial interest as they separate the hydrocarbons according to their size and reduce costs if the process is carried out at the same or similar temperature to that of the isomerization process [3,4].

Given the similar kinetic diameters of the C_6 isomers, listed in Table 1 [5–7], it is easy to predict that the separation of these isomers is a difficult process unless well-defined molecular sieves can be developed. Among the existing materials suitable for hydrocarbon separation, zeolites are probably the most studied, marketed, and commercially available, and currently used in the industry [1,8,9]. Metal-organic frameworks (MOFs) and carbon molecular sieves (CMSs) have also been developed and demonstrated to be appropriate for gas separation [2,10–14]. In addition, the possibility of using hierarchical materials for the separation of isomers has also been explored [2,10,12,14–23]; for example, the complex porous structure of micro-mesoporous carbons (MMCs) allows the adsorption of the smallest molecules, *e.g.* linear alkanes, in the micropores (< 2 nm) while the branched alkanes pass through the mesopores (between 2 and 50 nm) or macropores (> 50 nm) without being adsorbed [19].

Table 1. Kinetic diameters of the hexane isomers used in this study [5–7].

Hexane isomer (abbreviation)	Kinetic diameter (nm)
n-hexane (nHEX)	0.43
2-methylpentane (2MP)	0.50 – 0.54
2,2-dimethylbutane (22DMB)	0.62

In the field of gas separation, CMSs are usually synthesized by pyrolysis of polymers like polyacrylonitrile, poly(furfuryl alcohol), poly(vinylidene chloride), polyimide and its derivatives, and phenol-formaldehyde resins, among others [10,12]. On the other hand, eco-friendly synthesis methods have been proposed for producing MMCs using biomass or biosourced precursors instead of substances of petrochemical origin, thus avoiding the use of dangerous or toxic crosslinkers, catalysts, or solvents [24–27]. The synthesis of MMCs is mainly focused on tailoring the mesopore structure and this can be done by hard- or soft-template methods. In the first method, the mesoporous structure is an inverse replica of a hard template, commonly made from silica, which thus needs to be removed after the carbonization process. In the soft-template process, the carbon precursor polymerizes around a surfactant used as pore-directing agent, hence used as template, and then carbonization eliminates the surfactant, leading to the MMC [28]. Depending on the precursor/template pair selected, the complexity of the synthesis varies considerably. Tuning the size and morphology of the pores in MMCs allows efficient gas separation and other applications such as bio-sensing or energy storage [19,20,28–32]. In addition, a long and complex synthesis increases the cost of the MMC materials, questioning their potential industrial use.

Mimosa tannin (MT) extract is a mix of polyphenolic molecules derived from the bark of the *Acacia mearnsii* tree, which has been proven an excellent carbon precursor for the synthesis of not only MMCs, but also solid and hollow carbon microspheres, organic foams, and carbon gels [33]. Furthermore, it has been successfully demonstrated that tannin-derived nitrogen-doped MMCs are suitable for CO_2/N_2 gas separation and as preferential adsorbents of $C_2 – C_3$ alkynes over $C_2 – C_3$ alkenes and alkanes [34]. In this study, MT-derived MMCs are proposed

for use as molecular sieves for the separation of linear alkanes from their branched counterparts. MMCs were produced by a previously developed simple and green mechanosynthesis method [27], called surfactant-water-assisted mechanochemical mesostructuration (SWAMM). The SWAMM method requires mixing only MT extract, surfactant, and a little amount of water, thus being a fast and eco-friendly alternative to other synthesis methods that use hazardous and/or toxic substances and require long preparation times. By just changing the amounts of surfactant and water, either disordered mesoporous carbons (DMCs) with a worm-like mesostructure or ordered mesoporous carbons (OMCs) with a 2D hexagonal mesostructure can be produced. Such DMC and OMC materials have been characterized and tested as adsorbents to evaluate their selectivity towards the following hexane isomers: *n*-hexane (nHEX), 2-methylpentane (2MP), and 2,2-dimethylbutane (22DMB). Both types of MMCs are shown to exhibit good selectivity for the linear C_6 hydrocarbon. However, they demonstrate a completely different kinetic adsorption performance. These differences are attributed to the different connectivity of the mesoporous structure. In particular, for the OMC material, the narrow constrictions found at the mesopores entrance limit the adsorption of the mono-branched isomer, whereas the di-branched isomer is excluded from the inner porous structure, thus increasing considerably its separation selectivity under the studied conditions.

2. Materials and methods

Materials. MT extract supplied by Silva Chimica (St Michel Mondovi, Italy) and commercially available under the name Fintan OP was used as received as carbon precursor. It is composed of 80 to 82 % of phenolic flavonoids (mainly prorobinetinidin), 4 to 6 % of water, the rest being carbohydrate monomers and oligomers, as well as traces of amino acids. Pluronic® F127, a triblock copolymer composed of two hydrophilic chains (polyethylene oxide, PEO) and a hydrophobic chain (polypropylene oxide, PPO), was purchased from

Sigma-Aldrich and used as received. Pluronic® F127 forms micelles when dissolved in water, and has been used as pore-directing agent.

Synthesis of mesoporous carbons. The synthesis of ordered and disordered mesoporous carbons (OMCs and DMCs, respectively) was carried out by following a surfactant-water-assisted mechanochemical mesostructuration (SWAMM) method as detailed elsewhere [27]. In short, MT extract, Pluronic® F127 (P) and a small amount of water (W) were milled together in one step inside a planetary ball mill (Retsch, PM 100) with an agate bowl (50 mL) and balls (1 cm diameter) at a constant rotating speed (500 rpm) for 60 min. After milling, a paste was recovered and directly submitted to carbonization inside a tubular furnace using the following parameters: heating rate 1 °C min^{-1}, final temperature 900 °C, dwell time 1 h, and natural cooling. The whole process was carried out under a nitrogen flow of 100 mL min^{-1}. The MT:P:W mass ratio used during the synthesis was 2:0.75:1.75 g for producing the OMC, and 2:2:2 g for the DMC.

Chemical analysis. Elemental analysis (EA) was carried out using an Elementar Vario EL Cube analyzer to measure the bulk carbon, hydrogen, nitrogen, and sulfur contents. The oxygen content was measured independently with the same device but under different conditions. Regarding the surface chemistry, the composition was obtained with an ESCAPlus OMICROM system for X-Ray Photoelectron Spectroscopy (XPS) that comprises an analysis area of 1.75 × 2.75 mm^2 and a hemispherical electron energy analyzer. For the XPS analysis, the Mg X-Ray source (1253.6 eV) of the device was operated at 15 mA and 15 kV, survey scans were carried out using a pass energy of 50 eV and the high-resolution scans were acquired with a pass energy of 20 eV. Spectra were then analyzed with CASA software to calculate the atomic content of each element and the respective contributions of surface functional groups.

Morphology of the mesoporous structure. Transmission electron microscopy (TEM) images were acquired with a JEM – ARM 200F Cold FEG TEM/STEM equipped with a probe and

image spherical aberration correctors. The preparation of the samples consisted in dispersing the carbon powder in ethanol by low-power sonication, then a drop of the resultant suspension was deposited on a carbon-coated copper TEM grid (200 mesh) and left to dry in air before observation.

Textural characterization. The textural properties of the materials were studied through the physisorption of different probe molecules such as argon at -186 °C, nitrogen at -196 °C, and carbon dioxide at 0°C. These isotherms were measured on an Autosorb iQMP (Anton Paar Quantatec, Boynton Beach, FL) and a 3Flex manometric sorption analyzer (Micromeritics, Atlanta, GA). Prior to the measurement, both samples were outgassed at 150 °C for 12 h under turbo pump vacuum.

Calorimetric analysis. The evaluation of the heat of immersion of the DMC and OMC samples in the three liquid C_6 alkanes was performed in a Setaram C80D calorimeter operating at 30 °C. A full description of the experimental set-up can be found elsewhere [35]. Before the calorimetric experiment, the materials were outgassed at 200 °C for 24h in a specially designed glass reactor under ultra-high vacuum conditions. After the thermal treatment, the glass sample cell was sealed with a flame to maintain the sample under ultra-high vacuum conditions and introduced into the calorimetric chamber with the selected liquid. After stabilization of the thermal signal, the glass tip at the bottom of the sample cell was broken, and the heat released by the wetting of the sample by the C_6 probe molecule was recorded as a function of time. The enthalpy of immersion was then calculated from the area (integration) of the obtained peak.

Adsorption of alkanes. The tests were performed in a manometric system designed and manufactured by the LMA group at the University of Alicante and currently commercialized by Anton Paar (Quantachrome Instruments) under the name Vstar. Before the adsorption measurements, the samples were outgassed at 200 °C for 24h. The adsorption isotherms were performed at either 25 °C or 45 °C up to a relative pressure (p/p_0) of 1 for the three

adsorbates evaluated. It is important to highlight that the adsorption measurements were performed according to very strict equilibrium criteria (10 equilibrium points; interval time 15s; sorption rate limit 0.6666 Pa min^{-1}).

3. Results and discussion

3.1. Bulk and surface chemistry

Table 2 presents the bulk and surface chemical composition of DMC and OMC materials, measured by elemental analysis (EA) and X-ray photoelectron spectroscopy (XPS), respectively. It was found that oxygen (O) is the only relevant heteroatom present in the carbon structure since the nitrogen (N) content is very low and no sulfur (S) was detected. These findings are in good agreement with the composition of MT extract [36] and the fact that no doping treatment was carried out on the materials. Consistently, only O was detected on the surface of the carbon materials.

Table 2. Bulk and surface chemical composition of DMC and OMC, measured by elemental analysis (EA) and X-ray photoelectron spectroscopy (XPS), respectively.

Sample	EA					XPS	
	C (wt %)	H (wt %)	N (wt %)	S (wt %)	O* (wt %)	C (at %)	O (at %)
DMC	91.5	0.7	0.3	0.0	6.0	95.2	4.8
OMC	91.5	0.7	0.5	0.0	5.2	94.3	5.7

* Measured, difference to 100% is due to ash content

Figure S1 displays the high-resolution XPS spectra for carbon and oxygen (C1s and O1s, respectively) and the deconvoluted peaks representing the contributions of the different functional groups. All the corresponding values of binding energy and relative contributions are listed in Table S1. The O-II functionalities associated to phenolic groups have the highest contribution to the oxygen surface moieties, which is consistent with the polyphenolic nature of the molecules in MT extract used as carbon precursor. A contribution of ~20 % comes from the quinone- and carbonyl-type functionalities, *i.e.*, O-I groups. Finally, the carboxylic

groups or O-III have a contribution of ~7 % to the surface functionalities. From the elemental analysis, it is possible to conclude that DMC and OMC materials are chemically similar. Although the interaction and packing of n-alkanes on the surface of a carbon material have been shown to be favored by defects and heterogeneities [16,37,38], such small differences in the surface chemistry of the materials should have a minor effect on their separation performance.

3.2. Morphology of the mesoporous carbons

Transmission electron microscopy (TEM) images of DMC and OMC materials are shown in Figure 1. In agreement with the results previously reported for materials synthesized by the SWAMM method [32], the DMC exhibits a highly disordered worm-like mesopore structure (Figure 1a) whereas the OMC presents a 2D hexagonal structure (*p6mm* space group) with cylindrical mesopore channels, clearly recognized in the longitudinal and transversal views of the material shown in Figure 1b and 1c, respectively. Also from the TEM images, the pore size in the OMC can be roughly estimated to be between 5 and 7 nm.

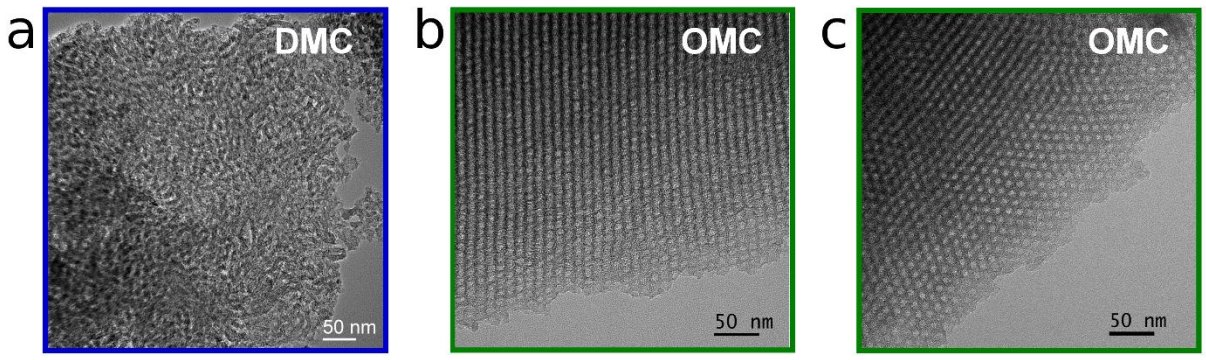

Figure 1. TEM images of: (a) the disordered mesoporous carbon (DMC); and (b) longitudinal and (c) transversal views of the ordered mesoporous carbon (OMC).

3.3. Textural properties

Figures 2a and 2b show the Ar and N_2 adsorption-desorption isotherms of DMC and OMC, respectively, which are combinations of type Ia, typical of ultramicroporous solids, and type IVa, characteristic of mesoporous materials where monolayer-multilayer adsorption is followed by capillary condensation [39]. Irrespective of the used adsorbate, all isotherms reveal "low-pressure hysteresis", which has been reported for some carbon materials and was associated with slow desorption kinetics due to an extremely tortuous micropore network or a possible swelling effect [40–42]. For the DMC and OMC samples, it can be seen that the observed low-pressure hysteresis is fully reproducible between consecutive sorption experiments on the same sample, *i.e.*, a potential deformation is also fully reversible for both materials, and the adsorption/desorption isotherms are fully repeatable (see Figure S2). Therefore, it is possible to carry out an application-targeted comparative textural analysis, where the derived values are considered as qualitative tools for comparison between DMC and OMC materials, rather than as an absolute assessment of these properties.

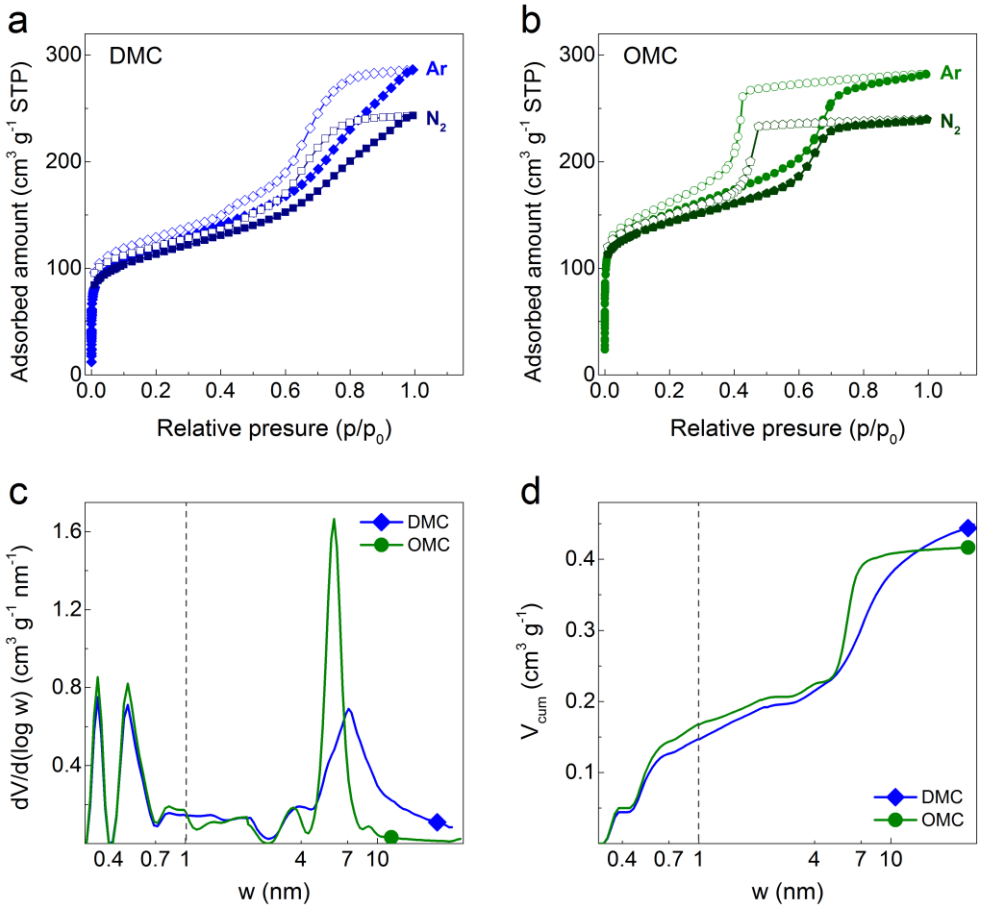

Figure 2. Argon (-186 °C) and nitrogen (-196 °C) adsorption-desorption isotherms for: (a) DMC and (b) OMC materials; the arrows mark the approximate onset of desorption in each case. Combined pore size distributions (PSDs) derived from the adsorption branches of argon and carbon dioxide isotherms (for w > 1 nm and w < 1 nm, respectively, separated by the dashed line), presented in (c) differential ($dV/d(log\ w)$) and (d) cumulated (V_{cum}) forms.

The combined pore size distributions (PSDs) in Figure 2c and the cumulative pore volumes in Figure 2d were obtained by applying a dedicated Ar -186 °C/carbon QSDFT kernel to the Ar adsorption branch and a dedicated CO_2/carbon 0°C NLDFT kernel to the CO_2 adsorption isotherm data for assessing ultramicropores in a reliable way [39,43]. The Ar-QSDFT kernel accounts for surface heterogeneities and takes quantitatively into account the delay in the condensation due to the existence of metastable adsorption film and hindered nucleation of liquid bridges [44–46]. The pore geometries of both samples were assumed as a slit/cylindrical hybrid pore model, *i.e.*, a slit pore model in the micropore range and a

cylindrical pore model for pores larger than 2 nm. The CO_2-NLDFT kernel assumes, similarly to the Ar-QSDFT kernel, a slit pore geometry in the micropore range.

Figures 2c and 2d clearly demonstrate the similarity of the PSDs in the ultramicroporous regime (< 0.7 nm) for both materials, which implies that they have similar microporous textures, due to the use of the same carbon precursor, the MT extract, for their synthesis. As shown in Figures 2a and 2b, the differences are essentially in the mesopore range, which is reflected in the different adsorption/desorption behaviors at higher relative pressures ($p/p_0 > 0.4$) and the corresponding PSDs (Figure 2c). The OMC exhibits a narrower PSD centered at ~6 nm while the DMC contains pores over a wider range of mesopores from 3 to 30 nm. From the Ar adsorption isotherms, the apparent BET areas (A_{BET}, calculated by applying the procedure described by Thommes et al. [39] and Rouquerol et al. [47]) are 379 and 487 $m^2\ g^{-1}$ for DMC and OMC, respectively. The micropore volume (V_μ) was found to be slightly higher for the OMC, but of similar magnitude to that of the DMC, *i.e.*, ~0.2 $cm^3\ g^{-1}$. This is consistent with previous studies that have shown that when pure MT extract is submitted to pyrolysis, the resultant carbon material is essentially microporous, with V_μ always around 0.2 ± 0.05 $cm^3\ g^{-1}$. In contrast, the DMC has a slightly higher mesopore volume (V_{meso}) than the OMC. The mesopores and their pore sizes can be developed by hydrothermal carbonization (HTC) treatments or by template methods, therefore V_{meso} can vary much more, depending on the synthesis method [32,48–52].

The textural analysis discussed so far already reveals that both samples are hierarchical micro-mesoporous materials. However, information on pore network connectivity can only be gained by a thorough comparison and analysis of their PSDs, obtained from both adsorption and desorption branches using different probe molecules such as Ar at -186 °C and N_2 at -196 °C. By identifying the mechanisms that control gas desorption/evaporation from the mesopores, it is possible to distinguish between freely accessible and constricted mesopores [53,54].

Figures 3b and 3e demonstrate that both probe molecules (Ar and N_2) yield the same PSD from the adsorption branch for DMC and OMC, respectively. Figure 3a compares the PSDs obtained from the adsorption and desorption of Ar for the DMC, for which the Ar-QSDFT metastable adsorption branch kernel was applied to the adsorption branch and the equilibrium transition kernel was applied to the desorption data. Hence, in the absence of pore networking effects (*e.g.*, pore blocking/percolation, cavitation), the PSD curves from adsorption and desorption branches should overlap [44,45]. Indeed, the PSDs derived from the Ar adsorption and desorption branches coincide over a wide range of pore sizes, but for the mesopore size range, deviations are observed. This indicates that a large portion of the mesoporous network in the DMC is freely accessible, while the other part of the mesopores can only be accessed through narrow necks. The type of constriction, *i.e.*, necks that lead to either pore blocking or cavitation-induced desorption/evaporation, can be distinguished by comparing the effects of the pore network on the adsorption of two different fluids, here N_2 and Ar. Figure 3b demonstrates very good agreement between Ar and N_2 PSDs obtained from the corresponding adsorption branches. The PSDs obtained from the desorption branches also show very good agreement over a wide range of pore sizes; however, differences are observed in the lower mesopore range, caused by cavitation-induced evaporation from a small fraction of the mesopores which can only be accessed through narrow pore necks. The size of these necks can be in ranges from micropores up to a critical width of *ca.* 5 – 7nm [53–55]. These results, combined with data from the comparison of the Ar adsorption and desorption branches, reveal a complex pore network structure with differently accessible mesopores within the DMC material. Based on the performed analysis, the majority of mesopores are freely accessible, while a small part of the mesopore network is accessible through narrow necks.

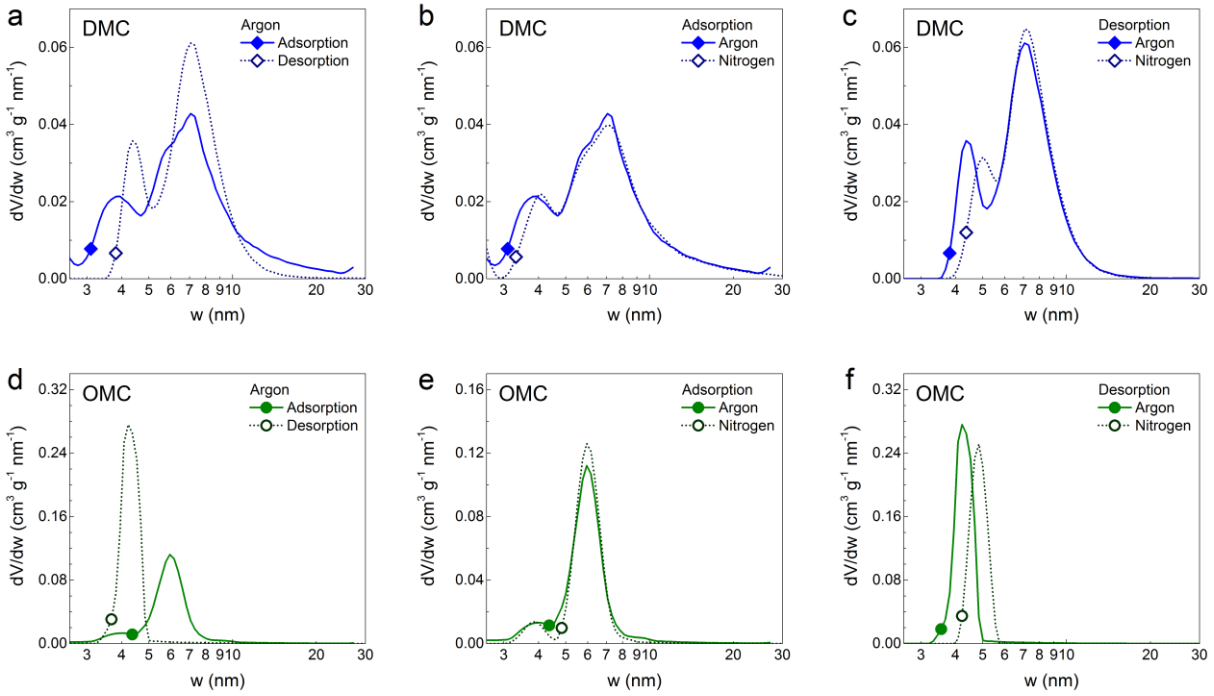

Figure 3. Pore size distributions (PSDs) in the mesopore range for (a, b, c) DMC and (d, e, f) OMC samples. (a, d) PSDs obtained from the adsorption and desorption branches of Ar isotherms. PSDs obtained from Ar and N_2 isotherms using their (b, e) adsorption branches and (c, f) desorption branches.

In contrast, for the OMC material, almost the whole mesopore network is only accessible through narrow constrictions. The existence of pore network effects such as pore blocking or cavitation for the underlying pore evaporation mechanism is confirmed by the disagreement of the PSDs obtained from the Ar adsorption/desorption branches, see Figure 3d. Moreover, the strong disagreement of the PSDs obtained from the Ar and N_2 desorption isotherms (Figure 3f) suggests that evaporation of condensed fluid from the complete mesoporosity of the OMC occurs mostly only by cavitation. As already discussed, in addition to its mesopore network, the OMC exhibits mainly ultramicropores with pore sizes of 0.35 and 0.5 nm and a small fraction of wider micropores (see Figure 2c). Hence, these micropores must be the entrances of the mesopores, which then lead to cavitation upon depletion of the mesopores. As OMC and DMC have similar textural properties in the microporous range (see Figure 2c), the micropores should also be responsible for the fraction of the mesopores that is emptied by

cavitation in the DMC material. The illustration of the different pore networks will be discussed below for both materials, together with the adsorption of different hexane isomers and their accessibility in the mesopores.

3.4. Immersion calorimetry

To evaluate further the accessibility of the C_6 isomers to the inner pores of OMC and DMC, immersion calorimetry measurements were performed using the three iso-alkanes nHEX, 2MP, and 22DMB in liquid phase. As can be appreciated in Table 3, the enthalpy of immersion, $-\Delta H_{imm}$, is the largest for the linear hydrocarbon, followed by the mono- and di-branched isomers. A slightly larger $-\Delta H_{imm}$ for nHEX was measured in the DMC. This can be ascribed to the better connectivity of the pore network that, compared to the OMC, allows better diffusion and provides a larger accessible area to the liquid. In addition, $-\Delta H_{imm}$ decreases as the kinetic diameter of the molecule increases for both DMC and OMC. However, a larger decrease in enthalpy is observed for 22DMB in the OMC. $-\Delta H_{imm}$ was used to calculate the surface area accessible to each C_6 isomer, *S*, by assuming that $-\Delta H_{imm}=S(-\Delta h_{imm})$, where $-\Delta h_{imm}$ is the areal enthalpy of immersion [35]. This method of calculation requires the use of a non-porous reference material, usually a carbon black, $-\Delta h_{imm}$ being characteristic of a specific solid-liquid system. Consequently, the accessible surface area for a given liquid in a target solid can be estimated provided that the sample and the reference share similar physicochemical characteristics [35,56,57]. For this study, carbon black V3G was used as the reference, having a surface area of 62 m^2 g^{-1} and $-\Delta h_{imm}$ values of 7.89 J g^{-1}, 7.42 J g^{-1}, and 6.73 J g^{-1} in nHEX, 2MP and 22DMB, respectively; the calculated values of *S* are also listed in Table 3. *S* values decrease as the kinetic diameter of the probe molecule increase; however, for the OMC, *S* decreases at a faster rate than for the DMC. The poor accessibility of 22DMB in the OMC sample indicates that the constrictions connecting its mesoporous

network are slightly wider than 0.5 nm, allowing partial access to 2MP and almost excluding 22DMB. On the contrary, the higher *S* values observed for the three C_6 isomers in the DMC corroborate that its pore network is connected by pores of more varied sizes, which improves the accessibility of the surface to even the largest probe molecule, *i.e.*, 22DMB. These results are in close agreement with the conclusions drawn from the textural characterization carried out by Ar, N_2, and CO_2 adsorption.

Table 3. Enthalpy of immersion ($-\Delta H_{imm}$) and accessible surface area (*S*) for the different C_6 isomers in samples DMC and OMC.

Sample	nHEX		2MP		22DMB	
	$-\Delta H_{imm}$ (J g^{-1})	*S* (m^2 g^{-1})	$-\Delta H_{imm}$ (J g^{-1})	*S* (m^2 g^{-1})	$-\Delta H_{imm}$ (J g^{-1})	*S* (m^2 g^{-1})
DMC	63.3	497	44.2	369	32.1	296
OMC	58.7	461	20.0	167	10.0	92

3.5. Adsorption of hexane isomers

The adsorption performance of DMC and OMC samples was evaluated for the three C_6 hydrocarbon isomers under study. Figure 4 shows the vapor adsorption isotherms for the C_6 isomers at 45 °C for the two evaluated samples. In general, the adsorption profile of the three isomers is similar for a given sample, with a certain amount adsorbed at low relative pressures, due to the presence of micropores, and a hysteresis loop at medium to high relative pressures, associated with the presence of mesoporosity. At this point, it is interesting to note that the shape of the hysteresis loop resembles that observed with Ar or N_2 at cryogenic temperatures, thus reflecting an analogous sensitivity of larger hydrocarbons to the size and shape of the mesopores during condensation.

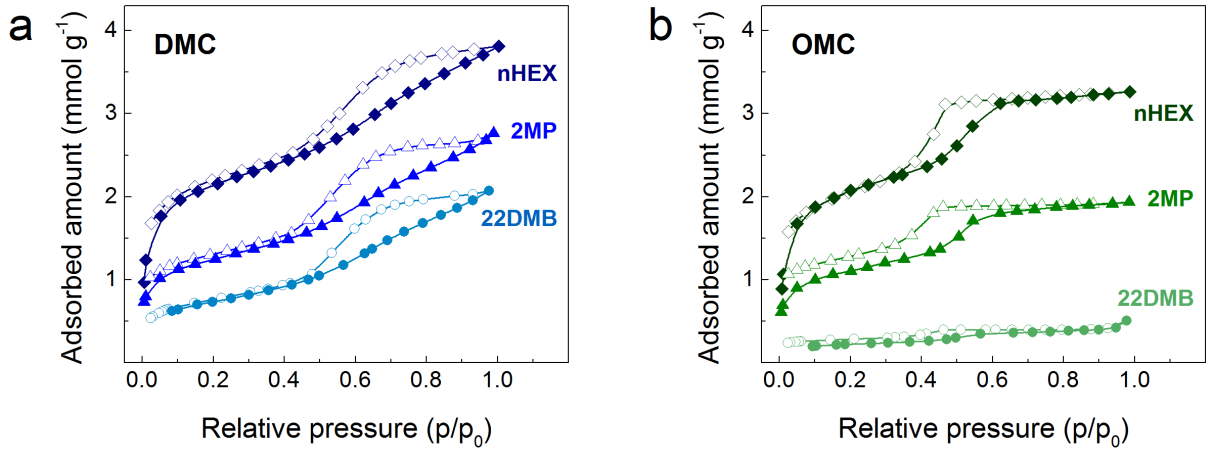

Figure 4. Vapor adsorption-desorption isotherms of nHEX, 2MP, and 22DMB for (a) DMC and (b) OMC materials, acquired at 45 °C.

The vapor adsorption of the C_6 isomers denotes important differences between DMC and OMC samples. Figures 4a and 4b show that nHEX is able to access the inner porous structure of both DMC and OMC. The uptakes at 45 °C, 3.8 and 3.3 mmol g^{-1} for the DMC and OMC, respectively, are comparable to those reported recently for nHEX adsorption in MOFs [58]. Figure 4a shows that in the DMC sample, nHEX has full access to the entire inner structure, whereas mono- and di-branched hydrocarbons have only partial access to the porosity with an uptake of 2.8 and 2.1 mmol g^{-1}, respectively. Indeed, increasing the molecule size reduces the accessible pore volume, while the hysteresis loop associated with condensation/evaporation in the mesoporous network has remained practically unchanged, *i.e.*, this indicates that the accessibility to the mesopore network characteristic of DMC is not completely limited, even for the bulkier 22DMB. Concerning the OMC sample, the scenario changes completely, the study of the vapor adsorption isotherms indicates a highly selective performance with respect to DMC as shown in Figure 4b. In the OMC, nHEX can access the inner porous structure, while the mono-branched C_6, 2MP, has limited access to the micro-mesopore network with an uptake of 1.9 mmol g^{-1}; the observed low-pressure hysteresis here may be due to slow kinetics due to existing pore constrictions. Finally, 22DMB is almost completely excluded as an uptake of only 0.5 mmol g^{-1} was measured.

All observations are in line with the results of the immersion calorimetry experiments discussed above (see Table 3) and the results of the advanced textural analysis. This is reflected in the schemes in Figure 5 that illustrates the connectivity of the porous structure of the DMC and OMC materials based on our advanced adsorption and calorimetric characterization results. Thus, the DMC material has pore bodies and necks of different sizes that would allow access of all the C_6 isomers (Figure 5a), to a greater or lesser extent, to micropores and mesopores. In contrast to the well-connected structure of the DMC, the OMC exhibits a pore structure with reverse hierarchy [59] where the uniform mesopores are mainly connected through narrow micropores of sizes around or below ~0.5 nm (Figure 5b). These notable differences in pore network connectivity would eventually lead to very different selectivity behavior of the materials, as shown below.

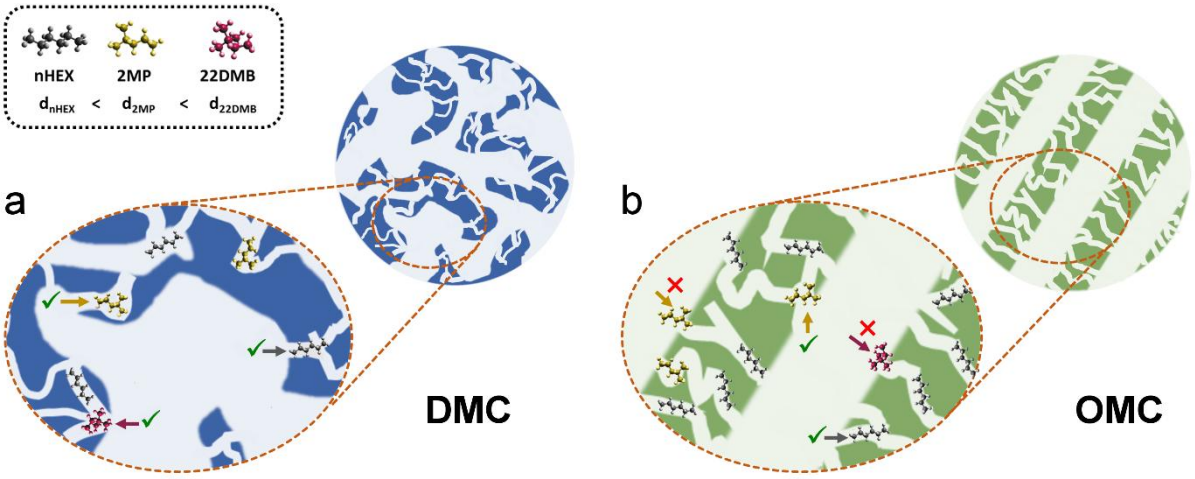

Figure 5. Scheme of the connectivity of the porous structure of (a) DMC and (b) OMC materials. The different kinetic diameters of the C_6 isomers ($d_{nHEX} < d_{2MP} < d_{22DMB}$) result in different accessibility of each molecule into the porous structure due to the presence of pore necks with similar or larger sizes.

3.6. Selectivity in the separation of C_6 isomers

The results described above for the materials tested as adsorbents for C_6 isomers were observed for single-component gases. However, industrial applications require the evaluation of adsorption performance in the case of gas mixtures, for which it is possible to assess the multi-component adsorption isotherms of the materials using the ideal adsorbed solution theory (IAST) [60]. Using the single-component adsorption isotherms as input data for IAST, the adsorbed amounts of each component from binary and ternary gas mixtures of nHEX, 2MP, and 22DMB (at 45 °C) in DMC and OMC materials were obtained. These data were then used to calculate the selectivity of nHEX (in binary mixtures) and nHEX+2MP (in ternary mixtures) shown in Figure S4 and Figure 6, respectively. The used methodology and the corresponding equations are described in detail in the Supplementary Information (SI).

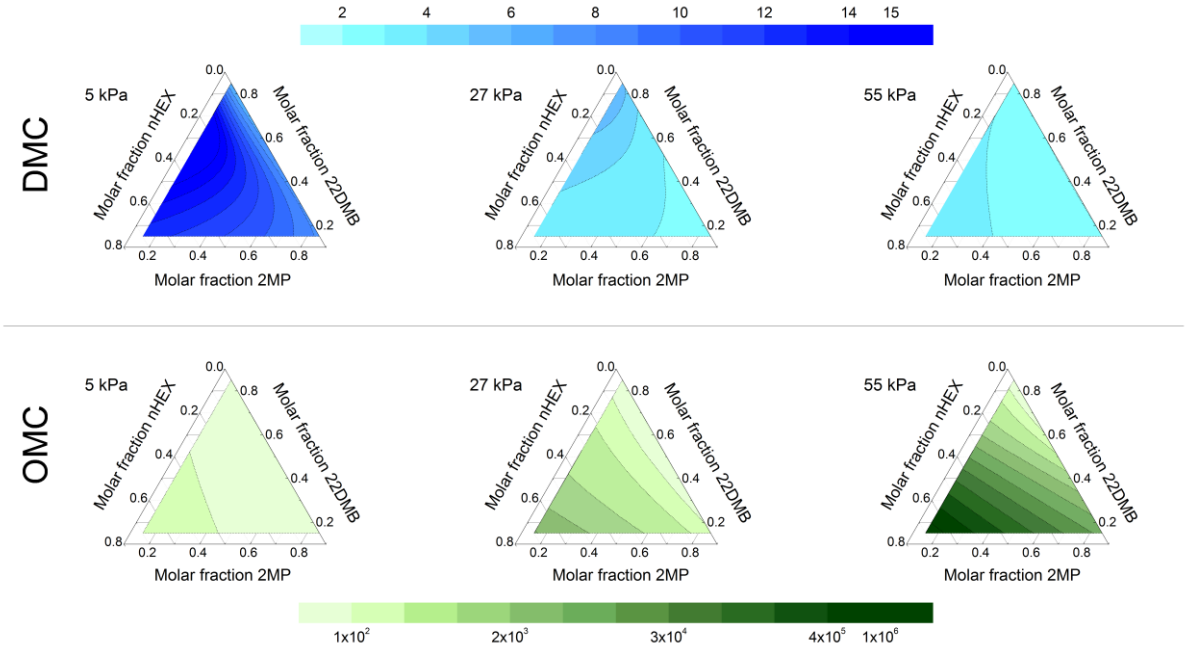

Figure 6. Selectivity of nHEX+2MP over 22DMB from ternary mixtures at 45 °C and different pressures for DMC and OMC materials.

For the ternary mixtures, Figure 6 (top) shows the adsorption selectivity of nHEX+2MP over 22DMB when increasing the pressure from 5 to 55 kPa for the DMC. The selectivity decreases as the pressure increases until reaching minimum values, between 2 and 3.7, at 55

kPa. Remarkably, for the OMC, the minimum values of selectivity of nHEX+2MP over 22DMB at the lowest pressure (5 kPa) are already around 40 and increase considerably with pressure, as shown in Figure 6 (bottom). Figures S4a and S4b show the selectivity of nHEX over the mono- and di-branched isomers in binary mixtures for the DMC. Note that, regardless of the amount of nHEX in the mixture, the values are higher at low pressures (< 20 kPa), where the effect of the larger kinetic diameter is more obvious. For higher pressures, the selectivity decreases considerably and remains almost constant at ~2 and ~4 for the nHEX+2MP and nHEX+22DMB mixtures, respectively. On the other hand, the OMC exhibits a relatively low selectivity in nHEX+2MP mixtures, with values between 1.5 and 3.8, as seen in Figure S4c. However, Figure S4d shows that for binary mixtures of nHEX+22DMB, a higher selectivity towards linear hydrocarbons is achieved, which increases with pressure and the percentage of nHEX in the mixture until values of the order of ~10^6 are reached. The high selectivity of the OMC in binary and ternary mixtures, especially those containing 22DMB, is a clear consequence of the narrow size of the constrictions connecting the mesoporous structure, very close to the kinetic diameter of 22DMB, resulting in the exclusion of the di-branched isomer from the material (see again Figure 5).

Previous studies described in the literature indicate that selectivity of linear/di-branched hydrocarbons close to infinity is difficult to achieve, except in some specific MOFs [61,62]. However, the high adsorption uptake, even at low relative pressures, and the high selectivity observed over the entire pressure range evaluated for the OMC, constitute one of the best results reported so far in the literature for this specific application [63–65]. Table S2 gathers some data on the adsorption performance of different materials such as carbons, zeolites, MOFs, and zeolitic imidazolate frameworks (ZIFs) tested for the separation of C_6 isomers compared to those of the tannin-derived MMCs of this study [4,20–22,58,65,66]. Even more, to directly compare the C_6 separation performance of the present MMCs derived from MT extract with that of MOFs used for gas separation, IAST calculations were performed using

the single-component adsorption isotherms of HKUST-1, UiO-66, and ZIF-8, previously reported by Cuadrado-Collados et al. [58]. Given the available data for the MOFs in the aforementioned study, in order to compare the performance consistently, the single-component adsorption isotherms of DMC and OMC were acquired at 25 °C (not shown) and IAST calculations were carried out using the adsorption branch instead of the desorption branch. From the multi-component isotherms obtained at 25 °C, the corresponding selectivity values were calculated; it should also be noted that HKUST-1 and UiO-66 have been reported to present a "reverse" hierarchy of adsorption, meaning that these MOFs have preferential adsorption of C_6 isomers in the order: di-branched > mono-branched > linear [58,65]. Therefore, the selectivity for materials with this type of hierarchy must be redefined as the inverse of the "normal" hierarchy observed for the MMCs materials of this study (see details in the SI).

Figure 7 shows the selectivity with respect to the corresponding amount of adsorbed gas, or capacity, of the materials in this study and the aforementioned MOFs. Figure 7a shows the selectivity for separating nHEX from an nHEX+2MP mixture, with nHEX/2MP molar ratios of 30/70, 50/50, and 70/30, versus the total capacity. For this nHEX+2MP binary mixture, UiO-66 has the lowest separation performance, DMC and OMC materials have similar performance, while ZIF-8 and HKUST-1 present the best performance with the highest values of both capacity and selectivity (see again Figure 7a). Figures 7b and 7c consider the selectivity for separating: (i) nHEX from a binary mixture of nHEX+22DMB with nHEX/22DMB molar ratios of 30/70, 50/50 and 70/30 (Figure 7b), and (ii) nHEX+2MP from a ternary mixture with (nHEX+2MP)/22DMB molar ratios of (15+15)/30, (25+25/50) and (35+35)/30 (Figure 7c). In cases (i) and (ii), the most significant performance improvement is observed for the OMC. Indeed, although the capacity of the OMC is moderate, Figures 7b and 7c show that its selectivity is at least 3 orders of magnitude higher than that of the rest of the

materials compared here, thus exhibiting superior performance in gas separation under the studied conditions.

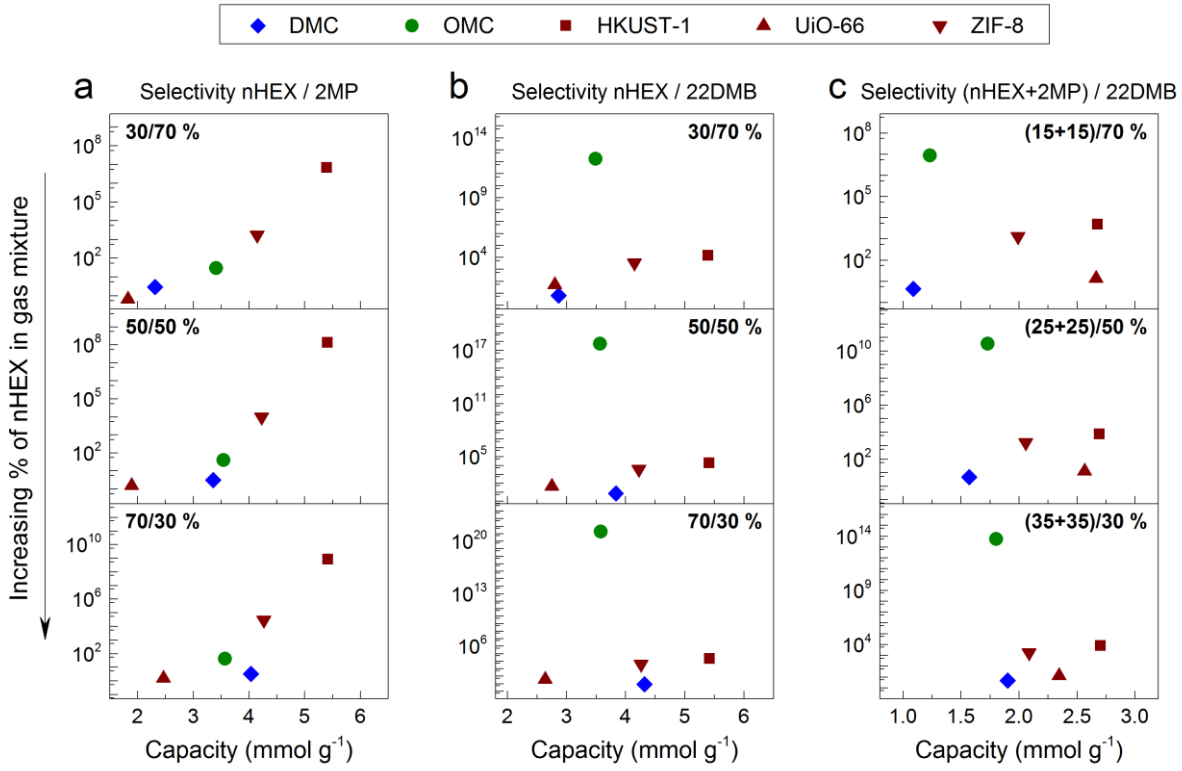

Figure 7. Selectivity versus capacity of DMC and OMC materials obtained from IAST compared to that of some metal-organic frameworks (MOFs), at 25 °C and 50 kPa, for (a, b) binary mixtures, and (c) ternary mixtures.

4. Conclusion

The surface and textural properties of two types of micro-mesoporous carbons (MMCs) derived from mimosa tannin (MT), a disordered mesoporous carbon (DMC) and an ordered mesoporous carbon (OMC), were characterized in detail by elemental analysis, X-ray photoelectron spectroscopy (XPS), advanced physisorption using different probe molecules (Ar, N_2, and CO_2) and immersion calorimetry. The combination of these techniques led to a detailed assessment of the key differences in the pore network characteristic of DMC and

OMC materials. The DMC was found to have a well-connected porous network with a wide pore size distribution (PSD) in the mesopore range, while the OMC displayed a narrower PSD in the mesopore range with highly restricted access through micropores. The single-component vapor adsorption of nHEX, 2MP, or 22DMB revealed that the MMCs exhibited a "normal" hierarchy of adsorption capacity in the order linear > mono-branched > di-branched, in good agreement with the results of immersion calorimetry. Besides, there was no evidence that the surface chemical composition had a significant impact on the adsorption of the C_6 isomers by the studied materials. Ideal adsorbed solution theory (IAST) calculations allowed demonstrating that the OMC exhibits a remarkably high selectivity (~10^6) for separating nHEX from binary mixtures of nHEX+22DMB and nHEX+2MP from ternary mixtures of nHEX+2MP+22DMB. To the best knowledge of the authors, such high values of selectivity have never been reported before for porous carbons, being even higher than those obtained with MOFs, some of which were directly compared to the materials synthesized here.

The results from this study clearly demonstrate that the unique pore structure of the OMC, where the complete mesopore network is exclusively accessible through ultramicropores, reflecting a perfect reverse hierarchy, is ideal for the described separation application of C_6 isomers, whereas the highly connected but disordered micro-mesopore network of the DMC is less suitable for hydrocarbon separation. Hence, this study shows that MMCs derived from MT have great potential to be used for selective separation of di-branched C_6 isomers, with the advantage of being produced by an easy, low-cost, and green synthesis method.

Acknowledgments

Jimena Castro-Gutiérrez gratefully acknowledges CONACYT-SENER for the scholarship awarded (601021/438978) to support her PhD studies, resulting in the work presented herein. This study was partly funded by the French PIA project "Lorraine Université d'Excellence", reference ANR-15-IDEX-04-LUE, and TALiSMAN project, funded by FEDER (2019-

000214). Joaquín Silvestre-Albero would like to acknowledge the financial support from MINECO (PID2019-108453GB-C21) and H2020 (MSCA-RISE-2016/NanoMed Project). Special thanks to Philippe Gadonneix for his help in the laboratory and with the EA measurements.

References

[1] G. Laredo, F. Trejo-Zarraga, F. Jimenez-Cruz, J. Garcia-Gutierrez, Separation of Linear and Branched Paraffins by Adsorption Processes for Gasoline Octane Number Improvement, CHENG. 5 (2013) 153–173. https://doi.org/10.2174/2211334711205030001.

[2] Z. Bao, G. Chang, H. Xing, R. Krishna, Q. Ren, B. Chen, Potential of microporous metal–organic frameworks for separation of hydrocarbon mixtures, Energy Environ. Sci. 9 (2016) 3612–3641. https://doi.org/10.1039/C6EE01886F.

[3] D.S. Sholl, R.P. Lively, Seven chemical separations to change the world, Nature. 532 (2016) 435–437. https://doi.org/10.1038/532435a.

[4] Z.R. Herm, B.M. Wiers, J.A. Mason, J.M. van Baten, M.R. Hudson, P. Zajdel, C.M. Brown, N. Masciocchi, R. Krishna, J.R. Long, Separation of Hexane Isomers in a Metal-Organic Framework with Triangular Channels, Science. 340 (2013) 960–964. https://doi.org/10.1126/science.1234071.

[5] A.F.P. Ferreira, M.C. Mittelmeijer-Hazeleger, M.A. Granato, V.F.D. Martins, A.E. Rodrigues, G. Rothenberg, Sieving di-branched from mono-branched and linear alkanes using ZIF-8: experimental proof and theoretical explanation, Phys. Chem. Chem. Phys. 15 (2013) 8795–8804. https://doi.org/10.1039/c3cp44381g.

[6] O.C. Gobin, S.J. Reitmeier, A. Jentys, J.A. Lercher, Role of the Surface Modification on the Transport of Hexane Isomers in ZSM-5, J. Phys. Chem. C. 115 (2011) 1171–1179. https://doi.org/10.1021/jp106474x.

[7] H.H. Funke, A.M. Argo, J.L. Falconer, R.D. Noble, Separations of Cyclic, Branched, and Linear Hydrocarbon Mixtures through Silicalite Membranes, Ind. Eng. Chem. Res. 36 (1997) 137–143. https://doi.org/10.1021/ie960472f.

[8] W. Vermeiren, J.-P. Gilson, Impact of Zeolites on the Petroleum and Petrochemical Industry, Top Catal. 52 (2009) 1131–1161. https://doi.org/10.1007/s11244-009-9271-8.

[9] S. Kulprathipanja, ed., Zeolites in Industrial Separation and Catalysis, Wiley-VCH, Great Britain, 2010.

[10] A. Ismail, L. David, A review on the latest development of carbon membranes for gas separation, Journal of Membrane Science. 193 (2001) 1–18. https://doi.org/10.1016/S0376-7388(01)00510-5.

[11] W.N.W. Salleh, A.F. Ismail, T. Matsuura, M.S. Abdullah, Precursor Selection and Process Conditions in the Preparation of Carbon Membrane for Gas Separation: A Review, Separation & Purification Reviews. 40 (2011) 261–311. https://doi.org/10.1080/15422119.2011.555648.

[12] S.M. Saufi, A.F. Ismail, Fabrication of carbon membranes for gas separation—a review, Carbon. 42 (2004) 241–259. https://doi.org/10.1016/j.carbon.2003.10.022.

[13] D. Peralta, G. Chaplais, A. Simon-Masseron, K. Barthelet, C. Chizallet, A.-A. Quoineaud, G.D. Pirngruber, Comparison of the Behavior of Metal–Organic Frameworks and Zeolites for Hydrocarbon Separations, J. Am. Chem. Soc. 134 (2012) 8115–8126. https://doi.org/10.1021/ja211864w.

[14] E. Adatoz, A.K. Avci, S. Keskin, Opportunities and challenges of MOF-based membranes in gas separations, Separation and Purification Technology. 152 (2015) 207–237. https://doi.org/10.1016/j.seppur.2015.08.020.

[15] Z.R. Herm, E.D. Bloch, J.R. Long, Hydrocarbon Separations in Metal–Organic Frameworks, Chem. Mater. 26 (2014) 323–338. https://doi.org/10.1021/cm402897c.

[16] G.FC. Laredo, J. Castillo, J.O. Marroquin, Gas-phase diffusion of linear and multi-branched alkanes on a carbon molecular sieve by the ZLC method, Separation and Purification Technology. 103 (2013) 36–42. https://doi.org/10.1016/j.seppur.2012.10.021.

[17] G.C. Laredo, J.L. Cano, J. Castillo, J.A. Hernandez, J.O. Marroquin, Octane enhancement by the selective separation of branched and linear paraffins in naphthas using a PVDC-PVC carbon molecular sieve, Fuel. 117 (2014) 660–666. https://doi.org/10.1016/j.fuel.2013.09.036.

[18] J. Pérez-Ramírez, Imagination has no limits, Nature Chem. 4 (2012) 250–251. https://doi.org/10.1038/nchem.1310.

[19] J.F. Vivo-Vilches, F. Carrasco-Marín, A.F. Pérez-Cadenas, F.J. Maldonado-Hódar, Fitting the porosity of carbon xerogel by CO2 activation to improve the TMP/n-octane separation, Microporous and Mesoporous Materials. 209 (2015) 10–17. https://doi.org/10.1016/j.micromeso.2015.01.010.

[20] J.F. Vivo-Vilches, A.F. Pérez-Cadenas, F.J. Maldonado-Hódar, F. Carrasco-Marín, C. Siquet, A.M. Ribeiro, A.F.P. Ferreira, A.E. Rodrigues, From Carbon Molecular Sieves to VOCs filters: Carbon gels with tailored porosity for hexane isomers adsorption and separation, Microporous and Mesoporous Materials. 270 (2018) 161–167. https://doi.org/10.1016/j.micromeso.2018.05.010.

[21] L.I. Devriese, L. Cools, A. Aerts, J.A. Martens, G.V. Baron, J.F.M. Denayer, Shape Selectivity in Adsorption of n- and Iso-alkanes on a Zeotile-2 Microporous/Mesoporous Hybrid and Mesoporous MCM-48, Adv. Funct. Mater. 17 (2007) 3911–3917. https://doi.org/10.1002/adfm.200700008.

[22] F. de Clippel, A. Harkiolakis, X. Ke, T. Vosch, G. Van Tendeloo, G.V. Baron, P.A. Jacobs, J.F.M. Denayer, B.F. Sels, Molecular sieve properties of mesoporous silica with

intraporous nanocarbon, Chem. Commun. 46 (2010) 928–930. https://doi.org/10.1039/B918864A.

[23] B. Yuan, X. Wu, Y. Chen, J. Huang, H. Luo, S. Deng, Adsorption of CO_2, CH_4, and N_2 on Ordered Mesoporous Carbon: Approach for Greenhouse Gases Capture and Biogas Upgrading, Environ. Sci. Technol. 47 (2013) 5474–5480. https://doi.org/10.1021/es4000643.

[24] Z. Gao, Y. Zhang, N. Song, X. Li, Biomass-derived renewable carbon materials for electrochemical energy storage, Materials Research Letters. 5 (2017) 69–88. https://doi.org/10.1080/21663831.2016.1250834.

[25] S. Herou, M.C. Ribadeneyra, R. Madhu, V. Araullo-Peters, A. Jensen, P. Schlee, M. Titirici, Ordered mesoporous carbons from lignin: a new class of biobased electrodes for supercapacitors, Green Chem. 21 (2019) 550–559. https://doi.org/10.1039/C8GC03497D.

[26] A.B. Fuertes, G.A. Ferrero, N. Diez, M. Sevilla, A Green Route to High-Surface Area Carbons by Chemical Activation of Biomass-Based Products with Sodium Thiosulfate, ACS Sustainable Chem. Eng. 6 (2018) 16323–16331. https://doi.org/10.1021/acssuschemeng.8b03264.

[27] J. Castro-Gutiérrez, A. Sanchez-Sanchez, J. Ghanbaja, N. Díez, M. Sevilla, A. Celzard, V. Fierro, Synthesis of perfectly ordered mesoporous carbons by water-assisted mechanochemical self-assembly of tannin, Green Chemistry. 20 (2018) 5123–5132.

[28] M. Inagaki, M. Toyoda, Y. Soneda, S. Tsujimura, T. Morishita, Templated mesoporous carbons: Synthesis and applications, Carbon. 107 (2016) 448–473. https://doi.org/10.1016/j.carbon.2016.06.003.

[29] Y. Zhou, L. Tang, G. Zeng, J. Chen, Y. Cai, Y. Zhang, G. Yang, Y. Liu, C. Zhang, W. Tang, Mesoporous carbon nitride based biosensor for highly sensitive and selective analysis of phenol and catechol in compost bioremediation, Biosensors and Bioelectronics. 61 (2014) 519–525. https://doi.org/10.1016/j.bios.2014.05.063.

[30] J. Castro-Gutiérrez, N. Díez, M. Sevilla, M.T. Izquierdo, J. Ghanbaja, A. Celzard, V. Fierro, High-Rate Capability of Supercapacitors Based on Tannin-Derived Ordered Mesoporous Carbons, ACS Sustainable Chem. Eng. 7 (2019) 17627–17635. https://doi.org/10.1021/acssuschemeng.9b03407.

[31] G. Lin, R. Ma, Y. Zhou, C. Hu, M. Yang, Q. Liu, S. Kaskel, J. Wang, Three-dimensional interconnected nitrogen-doped mesoporous carbons as active electrode materials for application in electrocatalytic oxygen reduction and supercapacitors, Journal of Colloid and Interface Science. 527 (2018) 230–240. https://doi.org/10.1016/j.jcis.2018.05.020.

[32] J. Zhu, J. Yang, R. Miao, Z. Yao, X. Zhuang, X. Feng, Nitrogen-enriched, ordered mesoporous carbons for potential electrochemical energy storage, Journal of Materials Chemistry A. 4 (2016) 2286–2292. https://doi.org/10.1039/C5TA09073C.

[33] V. Fierro, A. Sánchez-Sánchez, A. Celzard, Tannins as Precursors of Supercapacitor Electrodes, in: E. Rincón-Mejía, A. de las Heras (Eds.), Sustainable Energy Technologies, CRC Press, Boca Raton, Florida, USA, 2018: pp. 201–228.

[34] J. Zhao, W. Shan, P. Zhang, S. Dai, Solvent-free and mechanochemical synthesis of N-doped mesoporous carbon from tannin and related gas sorption property, Chemical Engineering Journal. 381 (2020) 122579. https://doi.org/10.1016/j.cej.2019.122579.

[35] J. Silvestre-Albero, Characterization of microporous solids by immersion calorimetry, Colloids and Surfaces A: Physicochemical and Engineering Aspects. 187–188 (2001) 151–165. https://doi.org/10.1016/S0927-7757(01)00620-3.

[36] G. Tondi, A. Petutschnigg, Middle infrared (ATR FT-MIR) characterization of industrial tannin extracts, Industrial Crops and Products. 65 (2015) 422–428. https://doi.org/10.1016/j.indcrop.2014.11.005.

[37] A. Speltini, D. Merli, E. Quartarone, A. Profumo, Separation of alkanes and aromatic compounds by packed column gas chromatography using functionalized Multi-Walled

Carbon Nanotubes as stationary phases, Journal of Chromatography A. 1217 (2010) 2918–2924. https://doi.org/10.1016/j.chroma.2010.02.052.

[38] E. Papirer, E. Brendle, F. Ozil, H. Balard, Comparison of the surface properties of graphite, carbon black and fullerene samples, measured by inverse gas chromatography, (1999) 10.

[39] M. Thommes, K. Kaneko, A.V. Neimark, J.P. Olivier, F. Rodriguez-Reinoso, J. Rouquerol, K.S.W. Sing, Physisorption of gases, with special reference to the evaluation of surface area and pore size distribution (IUPAC Technical Report), Pure and Applied Chemistry. 87 (2015). https://doi.org/10.1515/pac-2014-1117.

[40] A. Linares-Solano, F. Rodríguez-Reinoso, J.M. Martín-Martínez, J. de D. López-González, Adsorption of Hydrocarbons on Air-Reacted Activated Carbons. II. High and Low Pressure Hysteresis, Adsorption Science & Technology. 1 (1984) 317–327. https://doi.org/10.1177/026361748400100405.

[41] F. Rodríguez-Reinoso, J.M. Martín-Martínez, A. Linares-Solano, R. Torregrosa, Further Comments on Low Pressure Hysteresis in Activated Carbons: Effect of Preparation Method, in: F. Rodriguez-Reinoso, J. Rouquerol, K.S.W. Sing, K.K. Unger (Eds.), Studies in Surface Science and Catalysis, Elsevier, 1991: pp. 419–427. https://doi.org/10.1016/S0167-2991(08)61347-6.

[42] A.M. Volosin, S. Chen, D.-K. Seo, High-surface area mesoporous carbons from gel templating and inorganic-organic hybrid gel formation, Journal of Solid State Chemistry. 281 (2020) 121040. https://doi.org/10.1016/j.jssc.2019.121040.

[43] S.H. Madani, C. Hu, A. Silvestre-Albero, M.J. Biggs, F. Rodríguez-Reinoso, P. Pendleton, Pore size distributions derived from adsorption isotherms, immersion calorimetry, and isosteric heats: A comparative study, Carbon. 96 (2016) 1106–1113. https://doi.org/10.1016/j.carbon.2015.10.072.

[44] G.Yu. Gor, M. Thommes, K.A. Cychosz, A.V. Neimark, Quenched solid density functional theory method for characterization of mesoporous carbons by nitrogen adsorption, Carbon. 50 (2012) 1583–1590. https://doi.org/10.1016/j.carbon.2011.11.037.

[45] S. Dantas, K.C. Struckhoff, M. Thommes, A.V. Neimark, Phase Behavior and Capillary Condensation Hysteresis of Carbon Dioxide in Mesopores, Langmuir. 35 (2019) 11291–11298. https://doi.org/10.1021/acs.langmuir.9b01748.

[46] A.V. Neimark, Y. Lin, P.I. Ravikovitch, M. Thommes, Quenched solid density functional theory and pore size analysis of micro-mesoporous carbons, Carbon. 47 (2009) 1617–1628. https://doi.org/10.1016/j.carbon.2009.01.050.

[47] J. Rouquerol, P. Llewellyn, F. Rouquerol, Is the bet equation applicable to microporous adsorbents?, in: Studies in Surface Science and Catalysis, Elsevier, 2007: pp. 49–56. https://doi.org/10.1016/S0167-2991(07)80008-5.

[48] S. Schlienger, A.-L. Graff, A. Celzard, J. Parmentier, Direct synthesis of ordered mesoporous polymer and carbon materials by a biosourced precursor, Green Chem. 14 (2012) 313–316. https://doi.org/10.1039/C2GC16160E.

[49] F.L. Braghiroli, V. Fierro, A. Szczurek, N. Stein, J. Parmentier, A. Celzard, Hydrothermally treated aminated tannin as precursor of N-doped carbon gels for supercapacitors, Carbon. 90 (2015) 63–74. https://doi.org/10.1016/j.carbon.2015.03.038.

[50] F.L. Braghiroli, V. Fierro, J. Parmentier, A. Pasc, A. Celzard, Easy and eco-friendly synthesis of ordered mesoporous carbons by self-assembly of tannin with a block copolymer, Green Chem. 18 (2016) 3265–3271. https://doi.org/10.1039/C5GC02788H.

[51] A. Sanchez-Sanchez, M.T. Izquierdo, J. Ghanbaja, G. Medjahdi, S. Mathieu, A. Celzard, V. Fierro, Excellent electrochemical performances of nanocast ordered mesoporous carbons based on tannin-related polyphenols as supercapacitor electrodes, Journal of Power Sources. 344 (2017) 15–24. https://doi.org/10.1016/j.jpowsour.2017.01.099.

[52] T. Selmi, A. Sanchez-Sanchez, P. Gadonneix, J. Jagiello, M. Seffen, H. Sammouda, A. Celzard, V. Fierro, Tetracycline removal with activated carbons produced by hydrothermal carbonisation of Agave americana fibres and mimosa tannin, Industrial Crops and Products. 115 (2018) 146–157. https://doi.org/10.1016/j.indcrop.2018.02.005.

[53] M. Thommes, B. Smarsly, M. Groenewolt, P.I. Ravikovitch, A.V. Neimark, Adsorption Hysteresis of Nitrogen and Argon in Pore Networks and Characterization of Novel Micro- and Mesoporous Silicas, Langmuir. 22 (2006) 756–764. https://doi.org/10.1021/la051686h.

[54] K.A. Cychosz, R. Guillet-Nicolas, J. García-Martínez, M. Thommes, Recent advances in the textural characterization of hierarchically structured nanoporous materials, Chemical Society Reviews. 46 (2017) 389–414. https://doi.org/10.1039/C6CS00391E.

[55] M. Thommes, K.A. Cychosz, Physical adsorption characterization of nanoporous materials: progress and challenges, Adsorption. 20 (2014) 233–250. https://doi.org/10.1007/s10450-014-9606-z.

[56] M.T. Gonzalez, A. Sepulveda-Escribano, M. Molina-Sabio, F. Rodriguez-Reinoso, Correlation between Surface Areas and Micropore Volumes of Activated Carbons Obtained from Physical Adsorption and Immersion Calorimetry, Langmuir. 11 (1995) 2151–2155. https://doi.org/10.1021/la00006a050.

[57] R. Denoyel, J. Fernandez-Colinas, Y. Grillet, J. Rouquerol, Assessment of the surface area and microporosity of activated charcoals from immersion calorimetry and nitrogen adsorption data, Langmuir. 9 (1993) 515–518. https://doi.org/10.1021/la00026a025.

[58] C. Cuadrado-Collados, C.K. Rojas-Mayorga, B. Saavedra, M. Martinez-Escandell, J.M. Osiński, P.Z. Moghadam, D. Fairen-Jimenez, J. Silvestre-Albero, Reverse Hierarchy of Alkane Adsorption in Metal–Organic Frameworks (MOFs) Revealed by Immersion Calorimetry, J. Phys. Chem. C. 123 (2019) 11699–11706. https://doi.org/10.1021/acs.jpcc.9b01381.

[59] W. Schwieger, A.G. Machoke, T. Weissenberger, A. Inayat, T. Selvam, M. Klumpp, A. Inayat, Hierarchy concepts: classification and preparation strategies for zeolite containing materials with hierarchical porosity, Chem. Soc. Rev. 45 (2016) 3353–3376. https://doi.org/10.1039/C5CS00599J.

[60] A.L. Myers, J.M. Prausnitz, Thermodynamics of mixed-gas adsorption, AIChE J. 11 (1965) 121–127. https://doi.org/10.1002/aic.690110125.

[61] H. Wang, X. Dong, J. Lin, S.J. Teat, S. Jensen, J. Cure, E.V. Alexandrov, Q. Xia, K. Tan, Q. Wang, D.H. Olson, D.M. Proserpio, Y.J. Chabal, T. Thonhauser, J. Sun, Y. Han, J. Li, Topologically guided tuning of Zr-MOF pore structures for highly selective separation of C6 alkane isomers, Nat Commun. 9 (2018) 1745. https://doi.org/10.1038/s41467-018-04152-5.

[62] L. Peng, Q. Zhu, P. Wu, X. Wu, W. Cai, High-throughput computational screening of metal–organic frameworks with topological diversity for hexane isomer separations, Phys. Chem. Chem. Phys. 21 (2019) 8508–8516. https://doi.org/10.1039/C8CP07527A.

[63] P.S. Bárcia, D. Guimarães, P.A.P. Mendes, J.A.C. Silva, V. Guillerm, H. Chevreau, C. Serre, A.E. Rodrigues, Reverse shape selectivity in the adsorption of hexane and xylene isomers in MOF UiO-66, Microporous and Mesoporous Materials. 139 (2011) 67–73. https://doi.org/10.1016/j.micromeso.2010.10.019.

[64] T. Duerinck, R. Bueno-Perez, F. Vermoortele, D.E. De Vos, S. Calero, G.V. Baron, J.F.M. Denayer, Understanding Hydrocarbon Adsorption in the UiO-66 Metal–Organic Framework: Separation of (Un)saturated Linear, Branched, Cyclic Adsorbates, Including Stereoisomers, J. Phys. Chem. C. 117 (2013) 12567–12578. https://doi.org/10.1021/jp402294h.

[65] D. Dubbeldam, R. Krishna, S. Calero, A.Ö. Yazaydın, Computer-Assisted Screening of Ordered Crystalline Nanoporous Adsorbents for Separation of Alkane Isomers, Angew. Chem. Int. Ed. 51 (2012) 11867–11871. https://doi.org/10.1002/anie.201205040.

[66] Y. Ling, Z.-X. Chen, F.-P. Zhai, Y.-M. Zhou, L.-H. Weng, D.-Y. Zhao, A zinc(ii) metal–organic framework based on triazole and dicarboxylate ligands for selective adsorption of hexane isomers, Chem. Commun. 47 (2011) 7197. https://doi.org/10.1039/c1cc12253c.